A HYBRID SILICON-ON-GLASS (SOG) LATERAL MICRO-ACCELEROMETER WITH CMOS READOUT CIRCUITRY

Junseok Chae, Haluk Kulah, and Khalil Najafi

Center For Wireless Integrated MicroSystems
University of Michigan, 1301 Beal Avenue, Ann Arbor, Michigan 48109-2122
Email: najafi@umich.edu, Tel: (734) 763-6650, Fax: (734) 763-9324

ABSTRACT

A hybrid micro-accelerometer system consisting of a new bulk Silicon-On-Glass (SOG) lateral capacitive micro-accelerometer and a CMOS interface circuit is presented. The accelerometer has a 120μm-thick proof mass, 2.2mm × 3.0mm in size with 3.2μm sensing gap defined by DRIE. The circuit has a 95dB dynamic range, a low offset of 370μV and can resolve better than 75aF. The hybrid system has a measured sensitivity of 40mV/g and resolution of 100μg/√Hz.

Keywords: Inertial sensors, μg accelerometer, sigma-delta

INTRODUCTION

High precision micro-accelerometers are increasingly needed in applications such as inertial navigation, seismology, and micro-gravity measurements [1]. Capacitive micro-accelerometers have several advantages such as high sensitivity, stable dc-characteristics, low drift, low power dissipation, and low temperature sensitivity. One of the important requirements for accelerometers is acceleration resolution [2], which is output noise spectral density [$V/\sqrt{Hz}$] divided by sensitivity of a system [V/g] times bandwidth of operation [$\sqrt{Hz}$]. A few *out-of-plane* (z-axis) micro-accelerometers which provide 10's of μg resolution have been developed [3, 4]. In order to reduce noise and increase sensitivity, these sensors utilize full wafer thickness or multiple wafers bonded for their proof mass, and a thin sacrificial layer to form sensing gap. However, it is not feasible to implement these techniques to *in-plane* (x or y-axes) sensors that are sensitive to acceleration parallel to the sensor substrate because of the relatively large sensing gap. Although surface micromachined accelerometers can be integrated with interface electronics to improve performance, due to their small mass they typically have a noise floor 100μg-1mg/√Hz [5, 6]. In order to overcome this limit, bulk micromachined or SOI accelerometers utilizing DRIE technology have been developed [7, 8]. These accelerometers utilize 25-70μm thick single-crystal silicon proof mass to reduce overall system noise. Nevertheless, these accelerometers either do not provide high enough resolution to satisfy an inertial grade performance or have complicated fabrication process and large parasitics. In this paper we report a low noise, high sensitivity lateral bulk-silicon accelerometer, with a simple fabrication process, which is interfaced in a hybrid fashion with a custom-designed switched-capacitor readout circuit.

SENSOR DESIGN

Figure 1 shows the proposed lateral accelerometer structure. The accelerometer has a 120μm-thick proof mass that is suspended over a glass substrate. It is quite simple and utilizes the well-known lateral combs for sensing and force feedback, except that it has a very large proof mass and sense capacitance because of the large thickness of the device structure realized using DRIE.

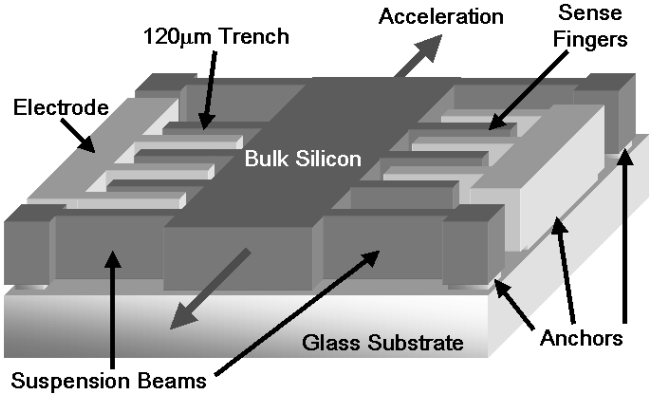

Figure 1. SOG lateral accelerometer

● *Performance optimization*

In order to achieve inertial-grade performance, an accelerometer is designed for maximum electrical sensitivity and minimum mechanical noise based on the allowable features of the process and device dimensions. One of the critical specifications that are required for inertial grade performance is μg resolution. Resolution is defined by two factors: noise floor and sensitivity. The total noise equivalent acceleration (TNEA) [$m/s^2\sqrt{Hz}$] is [9]

$$TNEA = \frac{\sqrt{4K_B TD}}{M}$$
$$D \propto n \cdot h\_sense^3 \cdot l\_sense / d_o^3 \qquad \text{Eq. 1}$$
$$M \propto t\_pm$$

where K_B is the Boltzmann constant, T is the temperature in kelvin, D is the damping coefficient, M is the mass of proof mass, n is the number of sense finger pairs, l_sense and h_sense is the length and height of the sense finger, respectively, d_o is the sensing gap distance, and t_pm is the thickness of the proof mass. For conventional lateral comb scheme, as shown above, D is heavily dependent on the height of the sense finger and the sensing gap distance.

The other factor determining the resolution is sensitivity [V/g], which has two components: sensitivity of

the sensor [*F/g*] and that of the readout electronics [*V/F*]. In sensor design phase, the sensitivity of readout electronics is not a variable parameter. Thus, only the sensitivity of the sensor is taken into account. The static sensitivity of the accelerometer can be expressed as:

$$Sensitivity = \frac{\Delta C_{static}}{a} = \frac{\varepsilon_o AM}{{d_o}^2 K} \qquad \textbf{Eq. 2}$$

where ε_o is the permittivity of air, A is sensing area, and K is spring constant. By using equations 1 and 2, we can define an object function (*Sensitivity / TNEA*) which is maximized to obtain the highest resolution.

$$\frac{Sensitivity}{TNEA} \propto \sqrt{\frac{l\_sense}{h\_sense}\frac{n}{K^2 \cdot d_o}} \cdot t\_pm^2 \qquad \textbf{Eq. 3}$$

As evident, there are only 6 parameters which contribute to the object function for conventional lateral comb drive accelerometers. Also Equation 3 clearly shows that increasing the thickness of the proof mass is more effective than changing the other parameters. However, as the thickness increases, it becomes more difficult to obtain a narrow and uniform gap between sense fingers, which is limited by the DRIE capability to achieve vertical etching profiles. Therefore, these 6 parameters are optimized under allowable features of the fabrication process and specifications of the sensor. The specifications of the sensor can be listed as mechanical dimensions, physical characteristics, and electrical properties. Mechanical dimensions are length and width of the proof mass, size of a die, etc. Physical characteristics are resonant frequency, cross axis sensitivity, quality factor, and shock resistance. Electrical properties are cut off frequency and sense capacitance. These 6 parameters are optimized by using MATLAB under various dependent parameters constrained by the specifications of the sensor. Figure 2 shows two optimization results. Here, the sensitivity is calculated with *TNEA* of 10μg/√Hz.

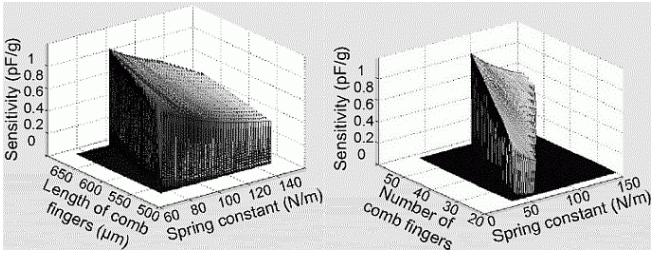

Figure 2. Parameter optimization

Table 1 summarizes the optimized design parameters. The design is made robust to accommodate process variations. The largest variation occurs during the DRIE process, while defining the sensing gap distance (d_o) and suspension beam width (*w_beam*). The variation affects sensitivity significantly since sensitivity is inversely proportional to ${d_o}^2$ and K, as shown in Equation 2, while Equation 4 shows that K is inversely proportional to ${w\_beam}^3$.

$$k \approx \frac{24EI}{{l\_beam}^3} = \frac{24E}{{l\_beam}^3} \times \left(\frac{t\_beam \cdot {w\_beam}^3}{12}\right) \qquad \textbf{Eq. 4}$$

where E is the Young's modulus, I is the moment of inertia, *l_beam* and *t_beam* are the length and thickness of the suspension beam, respectively.

Table 1. Micro-accelerometer design parameters

Mass of proof mass	0.5 milligram
Resonant frequency	2.14 kHz
Thickness of proof mass	120 μm
Sensing gap distance (d_o)	2.0 μm
Sense capacitance	32.1 pF
Spring constant of suspension beams	90.4 N/m
Length of sense finger	650 μm
Number of sense finger pairs	56
Cross axis sensitivity	< 0.1 %
Sensitivity / *TNEA*	(0.8 pF/g) / (10 μg/√Hz)

• Verification using FEM simulation

Since optimized parameters are calculated based on first order equations, FEM simulation (*ANSYS*) is used for further verification. Figure 3 shows the resonant frequencies of the micro-accelerometer. As can be seen the 1st mode resonant frequency is 2.14kHz, giving a spring constant of 93.5 N/m. The resonant frequencies for 2nd and 3rd modes are 14.6kHz and 22.9kHz, respectively, which are much larger than the 1st mode, resulting in low cross-axis sensitivity as expected.

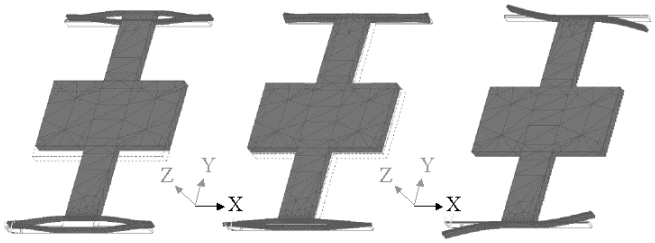

Figure 3. Resonant frequencies of a micro-accelerometer

Cross axis sensitivities for x-, and z-axes with respect to y-axis can be calculated using the following equation:

$$S_{a_x}^{a_y} = \frac{\Delta a_y / a_y}{\Delta a_x / a_x} = \frac{\Delta x_{1g}}{\Delta y_{1g}} \frac{(\Delta y_{2g} - \Delta y_{1g})}{(\Delta x_{2g} - \Delta x_{1g})}, \ (a_x = k_x \Delta x / m) \qquad \textbf{Eq. 5}$$

To determine the cross axis sensitivity, two-stage simulation is performed. First, a 1g acceleration is applied both on the sense axis (y-axis) and the x-axis, simultaneously. Next, 2g acceleration is applied on x-axis while maintaining the 1g acceleration on y-axis. Table 2 summarizes the deflections for each mode under these conditions. Cross axis sensitivities for x- and z-axes are calculated as -79dB and -75dB, respectively.

Table 2. Cross axis sensitivity. Note that y is the sense axis.

	Δx (nm)	Δy(nm)	Δz(nm)
1g for x & y axis	0.1411	54.490	0.0092
2g for x & 1g for y axis	0.2875	54.484	0.0094
1g for y & z axis	0.0045	54.502	1.1956
1g for y & 2g for z axis	0.0060	54.512	2.3962

Shock resistance is also simulated to evaluate if the device is robust enough against external unexpected shocks. Since proof mass movement is constrained for the sense axis, an external shock does not destroy the sensor. For x- and z-axes, a 1000g external shock is applied. The maximum stresses occur at the edge of the suspension beams as expected, which are 10.4MPa on x-axis, 98.6MPa on z-axis, respectively, as seen in Figure 4. Since the fracture stress for single crystal silicon is 7.0GPa, the results show that the sensor should be able to survive under a 1000g shock.

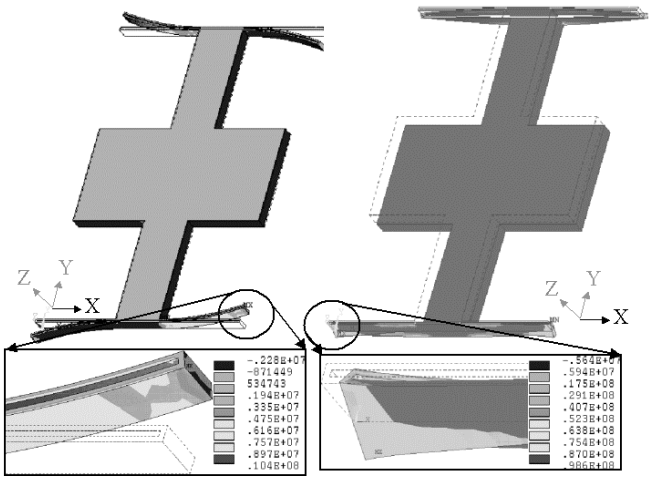

Figure 4. Stress distribution from an external shock

FABRICATION

The fabrication process has only 5-steps, requiring only 3 masks. Figure 5 shows the fabrication sequence. First, a glass substrate with a shallow recess is anodically bonded to a standard silicon wafer (Figure. 5 a, b). The silicon wafer is then thinned to 120μm using standard CMP (Figure. 5 c). Metal contacts are evaporated and patterned, and finally the wafer is DRIE etched to define the proof mass and sensing fingers (Figure. 5 d, e). This process is simple, requires no special steps other than DRIE, and does not require any high-temperature processing. The glass substrate is insulating which reduces parasitics, facilitating interfacing with a hybrid circuit.

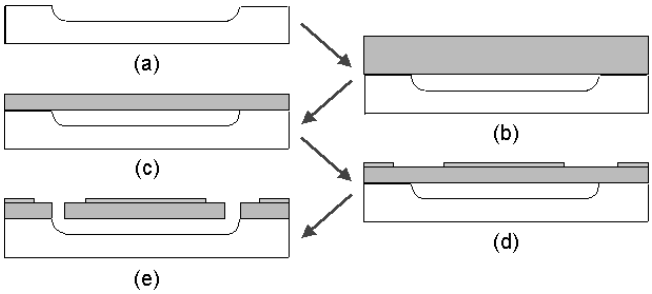

Figure 5. Fabrication sequence

Figure 6 shows SEM view of the accelerometer, and a close-up cross-sectional view of one of the sense fingers. The sensor dimensions are $2.2\times3.0\times0.12mm^3$. The fingers are ~100μm tall, and the sensing gap is ~3.2μm.

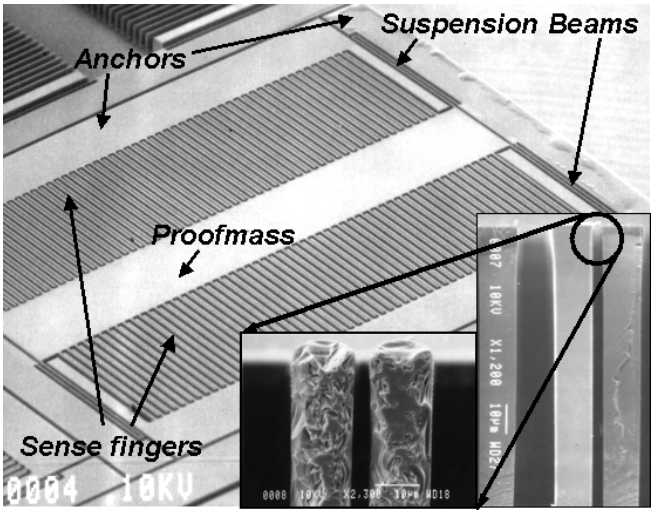

Figure 6. Top view of the accelerometer and cross section of the sense fingers

One of the problems in a DRIE process is micro-loading effect, which creates structures in different thickness for proof mass and sense fingers, resulting in reduced sensitivity. In addition to the loss of the thickness, the vertical etch profile is compromised. This causes non-linearity of the response of the accelerometer. In order to overcome this problem, before bonding the silicon wafer to the glass substrate, a shielding metal layer is deposited on the glass under the silicon in order to create the same electrical potential for both silicon and glass, preventing charging effect [10]. As a result, sense fingers have ideal vertical sidewall profile as seen in Figure 7.

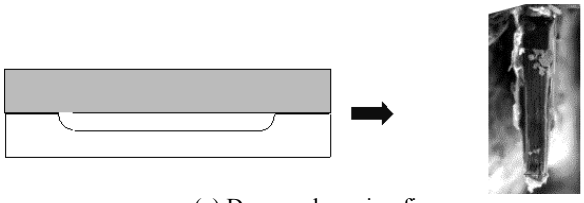

(a) Damaged sensing finger

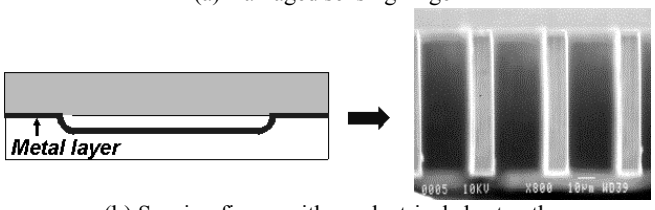

(b) Sensing finger with an electrical short path

Figure 7. Micro-loading effect

HYBRID SYSTEM-TEST & MEASUREMENTS

Capacitance changes from the micro-accelerometer are read out by a Σ-Δ switched-capacitor circuit [11], which can operate either in open- or closed-loop. The circuit includes chopper stabilization and correlated double sampling to cancel 1/f noise, amplifier offset and compensate for finite amplifier gain. It has 95dB dynamic range, an offset of 370μV and can resolve better than 75aF. Figure 8 shows the block diagram of the CMOS capacitive interface chip and its hybrid connection to the sensor. Two fixed external

reference capacitors are used to establish a full-bridge scheme.

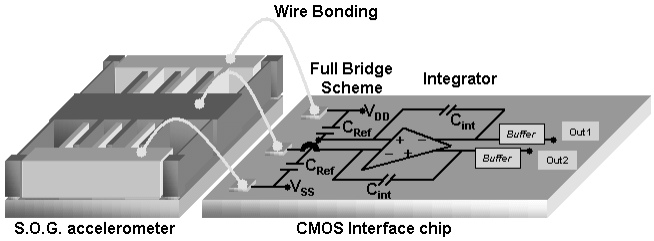

Figure 8. Hybrid accelerometer/circuit system

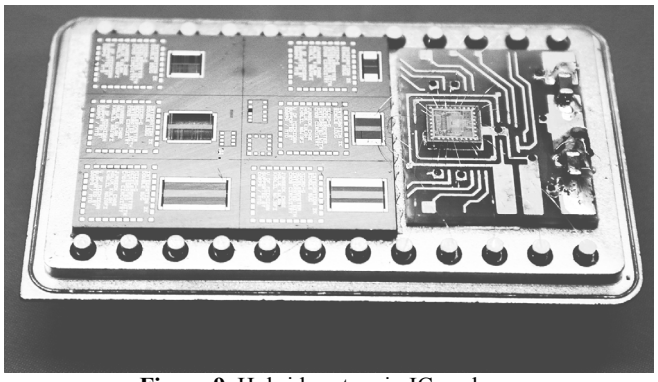

Figure 9. Hybrid system in IC package

Figure 9 shows the hybrid system assembled onto a PC board and mounted in a standard 24-pin IC package. The sensor and the interface circuit are packaged close to each other to minimize the parasitics. Note that the sensor die includes several devices and only one is connected to the readout circuit.

The hybrid system has been tested for sensitivity and resolution in open-loop configuration. The open-loop tests have been performed on a dividing head, in a 1g gravitational field, by changing the acceleration on the sensor from -1g to +1g. The sensor has a measured open-loop sensitivity of ~140fF/g, which is lower than expected because of the larger sensing gap distance (*3.2μm*) than designed (*2.0μm*). Figure 10 shows the open-loop test results for the hybrid system with respect to acceleration indicating a sensitivity of ~40mV/g. This result matches with the expected value since the readout circuit itself has a voltage gain of 330mV/pF. Noise floor of the system is measured using a dynamic signal analyzer HP3561. Figure 11 shows the measured output noise spectrum of the complete module with a dc input of 1g showing a noise floor better than 100μg/√Hz.

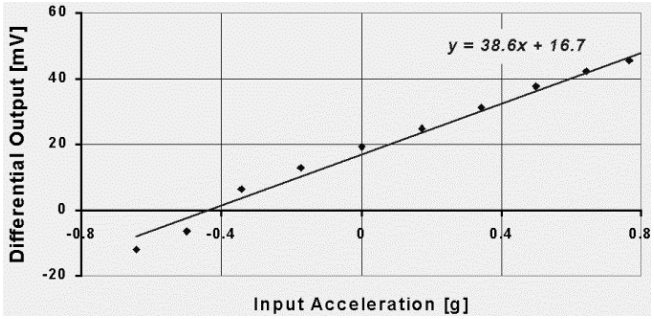

Figure 10. Open-loop test result of the hybrid system

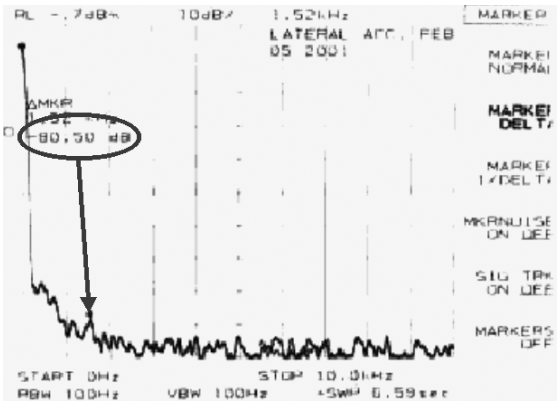

Figure 11. Output spectrum of the sensor/circuit module

DISCUSSION

Resolution of the hybrid system can be improved by increasing the circuit gain with laser trimming the integration capacitances. Moreover, from Equation 6, resolution could be further improved by a factor of 4 when thickness of proof mass increases to a full wafer thickness, while maintaining etching aspect ratio (120μm/3.2μm).

$$\frac{Sensitivity}{TNEA} \propto \left(\frac{t\_pm^3}{d_o} \right)^{1/2} \qquad \textbf{Eq. 6}$$

ACKNOWLEDGMENTS

The authors would like to thank Junmo Kang, Arvind Salian, and the staff at WIMS, University of Michigan. This work has been supported by DARPA under contract F30602-98-2-0231.

REFERENCES

[1] N. Yazdi, F. Ayazi, and K. Najafi, "Micromachined Inertial Sensors," *Proc. of IEEE*, vol. 86, pp. 1640-1659, 1998.

[2] "IEEE standard specification format guide and test procedure for linear, single-axis, nongyroscopic accelerometers," *IEEE Std. 1293-1998*, pp. 15, 1999.

[3] N. Yazdi and K. Najafi, "An all-silicon single wafer fabrication technology for presicion micro-accelerometers," *(Transducers'97)*, pp. 1181-1184, 1997.

[4] F. Rudolf, et al., "Precision accelerometers with μg resolution,"*Sensors Actuators*,vol.A21/A23,pp.297-302, 1990.

[5] Analog Devices, "High accuracy +-1g to +-5g single axis *i*MEMS accelerometer with analog input," datasheet, 1999.

[6] C. Lu, M. Lemkin, and B. Boser, "A monolithic surface micromachined accelerometer with digital output," *IEEE J. Solid-State Circuits*, vol. 30, pp. 1367-1373, 1995.

[7] Z. Xiao, et al., "Laterally capacity sensed accelerometer fabricated with anodic bonding and high aspect ratio etching," *(Transducers'99)*, 1999.

[8] M. Lemkin, et al., "A low-noise digital accelerometer using integrated SOI-MEMS technology," *(Transducers'99)*, pp. 1294-1297, 1999.

[9] T. B. Gabrielson, "Mechanical-thermal noise in micromachined acoustic and vibration sensors," *IEEE Trans. Electron Devices*, vol. 40, pp. 903-909, 1993.

[10] M. Chabloz, et al., "A method to evade microloading effect in deep reactive ion etching for anodically bonded glass-silicon structures," *(MEMS'00)*, pp. 283-287, 2000.

[11] N. Yazdi and K. Najafi, "An interface IC for a capacitive silicon μg accelerometer," *(ISSCC'99)*, pp. 132-133, 1999.